Investigation of residual stresses in planar dissimilar magnetic pulse welds by neutron diffraction

Marie-Noëlle Avettand-Fènoël, T. Sapanathan, T. Pirling, Guillaume Racineux, A. Simar, J.-M. Drezet

Investigation of residual stresses in planar dissimilar magnetic pulse welds by neutron diffraction

M.-N. Avettand-Fènoël[1,*], T. Sapanathan[2], T. Pirling[3], G. Racineux[4], A. Simar[2], J.-M. Drezet[5]

[1] Univ. Lille, CNRS, INRAE, Centrale Lille, UMR 8207 – UMET – Unité Matériaux et Transformations, F-59000 Lille, France
[2] UCLouvain, Institute of Mechanics, Materials and Civil Engineering, IMAP, B-1348 Louvain La Neuve, Belgium
[3] Institut Laue Langevin, 71 avenue des Martyrs, CS 20156, 38042 Grenoble, France
[4] Institut de Recherche en Génie Civil et Mécanique, UMR CNRS 6183, Ecole Centrale de Nantes, 44321 Nantes, France
[5] Ecole Polytechnique Fédérale de Lausanne, Institut des Matériaux, Station 12, 1015 Lausanne, Switzerland

* Corresponding author, e-mail: Marie-Noelle.Avettand-Fenoel@univ-lille.fr
Tel: 33(0)320436927, Fax: 33(0)320434040

Abstract

Residual stresses are investigated for the first time in a dissimilar AA1050 – DP450 steel magnetic pulse weld using neutron diffraction. Close to the joint interface, tensile residual stresses are observed in the Al sheet and compressive residual stresses are identified in the steel sheet. At the interface, longitudinal tensile stresses are dominant on the aluminum side and transverse and normal stresses show similar behavior. On the steel side, normal stresses remain small, and longitudinal and transverse residual stresses have a similar trend. It was identified that close to this tensile region in aluminum, residual stresses in steel become more compressive. These residual stress distributions essentially result from (i) the respective yield strengths of Al and steel and (ii) the high strains and high strain rates borne by both alloys due to the impact of the Al flyer sheet on the steel sheet during the process. The asymmetrical shape of the rectangular joint line entailed a lower magnitude of residual stresses along the short side of the weld.

Keywords

Magnetic pulse welding; dissimilar welding; residual stresses; neutron diffraction; interface

1. Introduction

Residual stresses generated by welding processes are detrimental to the performances and the service-life of welded structures since they can affect their strength, fatigue life, local strain localization as well as their surface integrity **[1-3]**. However, residual stresses are unavoidable and are expectedly larger in dissimilar joints compared to similar ones, due to the difference in crystal structures, microstructures, thermal properties and mechanical behaviors of the joined materials. Residual stresses generally accommodate in the weld due to thermal history, and strain and stresses experienced by the workpieces during the welding cycle. It is thus important to measure or estimate the residual stresses to eventually consider stress-relief treatments, such as annealing **[4]**, treatment under magnetic field and pulse current **[5]**, shot peening **[6]** etc. Such treatments either reduce residual stresses or change tensile residual stresses into less harmful compressive ones.

Residual stresses can be measured using different techniques (see review papers Ref. **[7-8]** for more details). These include destructive methods (sectioning techniques, contour method), semi-destructive methods (hole-drilling, ring-core, deep-hole) and non-destructive methods, such as Barkhausen noise, ultrasound, X-ray- and neutron diffraction **[9]**. X-ray and neutron diffraction are complementary methods. The advantages of neutron diffraction are the high penetration power of neutrons combined with a near 90° scattering geometry, allowing full stress tensor determination. The spatial resolution can be tuned for near interface measurements **[7].**

Only few studies measured residual stresses by neutrons **[10-11]**, X-rays **[12]** or synchrotron radiation **[3]** or hole drilling **[2,13-14]** in dissimilar joints obtained by fusion processes such as friction melt bonding **[10],** arc-assisted laser welding-brazing **[12]** or semi-solid like explosive welding **[2-3,11,13-15]**. Table 1 summarizes available literature measurements of

residual stresses in dissimilar welded joints. In Al alloy – steel joints obtained by friction melt bonding and arc-assisted laser welding-brazing, overall tensile residual stresses are associated to solidification shrinkage **[10]**. For explosive welds, the different nature of residual stresses in the flying and clamped sheets (Table 1) must have a correlation to the set-up and to the respective material properties such as, mechanical behavior, yield strength, coefficient of thermal expansion, possible accommodation of large strains according to their number of slip systems, etc.

Table 1: Residual stresses in dissimilar joints.

Fusion or solid-state process	Process	Alloys welded	Yield strength (MPa) *	Coefficient of thermal expansion ($°C^{-1}$) at 20°C *	Measurement method of residual stresses	Features of residual stresses close to the interface	Reference
Fusion	Friction melt bonding	Al alloy DP 600 steel grade	33-37 (annealed) 157-173 (hard) 330-440 **[16]**	22.9-24.1×10^{-6} 12.3×10^{-6} **[16]**	Neutron diffraction	Tensile in the joint	**[10]**
	Arc-assisted laser welding-brazing	5A06 Al alloy ST04Z galvanized steel	160 - 240	20×10^{-6} - 11 ×10^{-6}	X-ray diffraction	Tensile in the joint	**[12]**
Semi-solid	Explosive welding	Nb - 316L stainless steel (pipe)	75-105 170-310 **[16]**	7-7.2×10^{-6} 15-18×10^{-6} **[16]**	Neutron diffraction	Tensile in Nb external piece and compressive in internal steel piece	**[11]**
		Al - Cu - Al	24-26 28-40 **[16]**	22.9-24.1×10^{-6} 16.8-16.9×10^{-6} **[16]**	Hole drilling	Tensile in Al flying piece	**[2]**
		Ti grade 1 - S355J2 steel grade	189-215 382-395	8.5-9.3×10^{-6} 11.5-13×10^{-6} **[16]**	Hole drilling	Tensile in Ti flying piece	**[13-14]**
		Ti grade 2 - Al 1050	276-360 33-37 (annealed)	8.5-9.3×10^{-6} 22.9-	High energy X-ray diffraction (synchrotron radiation source)	Compressive in Ti flying sheet and unstressed	**[3]**

			157-173 (hard) **[16]**	24.1×10^{-6} **[16]**		Al	
		Ni - 304 stainless steel grade	125-160 190-310 **[16]**	12-13.5×10^{-6} 16-18×10^{-6} **[16]**	Finite elements method using measured strain distribution	Tensile in both materials	**[15]**
Solid-state	Rotary friction welding	AA7020 Al alloy – 316L stainless steel	299-352 170-310 **[16]**	22.7-23.9×10^{-6} 15-18×10^{-6} **[16]**	Neutron diffraction	Tensile on Al side and compressive on steel side	**[17]**

* For the yield strength or the coefficient of thermal expansion which are not reported in the papers, ranges of expected values are extracted from the software "Granta Edupack" **[16].**

Residual stresses appear to be generally high in fusion dissimilar welds due to solidification shrinkage **[3,15]**. Solid-state welding processes are thus appropriate as they avoid this shrinkage issue. Magnetic pulse welding (MPW) is one of these promising solid-state processes. It is a high-velocity impact welding process like gas gun welding, explosive welding, vaporizing foil actuator welding and laser impact welding **[18]**. MPW is an environmentally friendly process based on high speed electromagnetic forming at room temperature. It is particularly suitable to join dissimilar materials since it entails low peak temperatures for a few microseconds **[19-21]**. Previous studies of the authors considered welding of AA1050 aluminum alloy and DP450 dual phase steel and focused on the microstructural and mechanical characterization of a spot planar magnetic pulse joint made of these distinct materials **[22-23]**. Till date, only scarce studies on residual stresses in solid state dissimilar joints are reported in literature. Gan *et al.* measured residual stresses by neutron diffraction in an AA7020 aluminum alloy - 316L steel rotary friction weld near the bond line. They found tensile residual stresses on the Al side and compressive ones on the steel side **[17]**. However, according to the authors' knowledge, no study reports the analysis of residual stresses in magnetic pulse joints while the topic is of interest. Indeed, according to Raoelison

et al., the shrinking of the flyer plate prior to the interfacial collision is expected to relax residual stresses and would then lead to fracture of the joint interface during sample machining **[24]**. The present paper thus aims for the first time to unravel the residual stresses measured by neutron diffraction in an AA1050 aluminum alloy – DP450 steel dissimilar magnetic pulse weld.

2. Experimental procedure

The base materials are 40 mm wide sheets of AA1050 aluminum (150 mm long and 0.8 mm thick, hardness of 40 $HV_{0.05}$) and cold rolled DP450 steel (150 mm long and 1.2 mm thick, hardness of 160 $HV_{0.05}$). Their chemical compositions are reported in Table 2. Since the electrical conductivity of aluminum is higher than that of the DP steel, it constitutes the flyer sheet whereas steel becomes the target workpiece. A hump was deep drawn in the Al flyer sheet and its geometry is provided in Fig. 1a. The sheets were cleaned with acetone, then stacked with an overlapping length of 50 mm and finally joined by MPW with a discharge energy of 10 kJ. The generator presents a capacitor bank with a capacitance of 408 µF, an inductance of 100 nH and a resistance of 3 mΩ. The detailed geometry of the I-shaped Cu inductor is provided in Fig. 1b. This Cu inductor presents a 44 nH inductance and a 0.1 mΩ resistance. A 0.1 mm thick insulating sheet is inserted at the Al – inductor interface. Then, the stand-off distance corresponds to the hump depth of 1.5 mm. A schematic illustration showing the assembly view of the Al flyer, the steel and the Cu inductor before welding is given in Fig. 1c. For further details on the set-up, the reader can refer to **[25]**.

Table 2: Chemical composition of the base materials used in the MPW.

wt.%	Al	Fe	Si	Cu	Mn	Mg	Zn	Ti	C	Cr	Mo
AA1050	99.5	0.40	0.25	0.05	0.05	0.05	0.07	0.05	-	-	-
DP450 steel	0.015 - 0.08	balance	0.400 max	-	1.600 max	-	-	Ti+ Nb 0.050 max	0.100 max	0.800 max	0.300 max

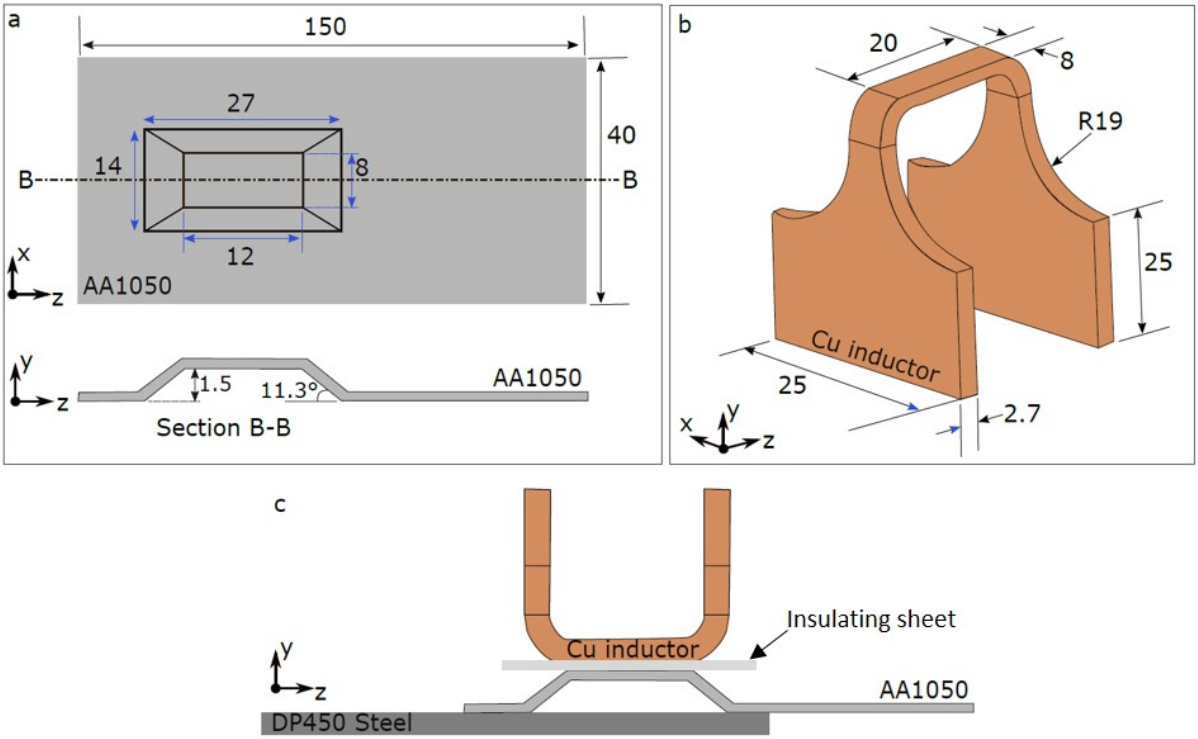

Fig. 1: (a) Geometry of the hump in the AA1050 flyer plate, (b) "I" shaped Cu inductor and (c) an assembly view showing the Al plate, DP steel and Cu inductor before the welding process. All dimensions are given in mm.

The residual stress measurements were carried out at the SALSA (Strain Analyser for Large and Small scale engineering Applications), a monochromatic stress diffractometer **[26]** at the Institut Max von Laue – Paul Langevin in Grenoble (France). The sound joint presents two long and two short weld lines (red rectangle in Fig. 2a). The microstructural observations were made on the cross-section along A-A using scanning electron microscope (SEM) under secondary electrons mode (Fig. 2c) and a light microscope (Fig. 2d and e). Fig. 2c exemplifies the aspect of the joint line while Fig. 2d and e prove that the spot joint center at the intersection of sections A-A and B-B is not welded. In Fig. 2d and e, the gap between the two plates occurs due to the 'jet' generated during the impact of the flyer plate. The jet cleans up the local surface of the plates where the welded lines are generated. The oxides and impurities ejected from the welded area have been accumulated at the interface where a gap can be observed meaning that, at that location, the plates are thus not welded (Fig. 2d). Since the

joint is relatively thin (Fig. 2), both materials have been investigated in the same measuring configuration (Fig. 3). The selected diffraction peaks for AA1050 and steel were those corresponding to the $\{311\}_{Al}$ and $\{211\}_{Fe}$ planes, respectively as suggested by Jacques *et al.* **[27]** and Chobaut *et al*. **[28]**. The neutron wavelength was set to 0.17026 nm, leading to diffraction angles 2θ of around 88.4° for the Al(311) reflection and 93.4° for Fe(211) (See Fig. 3 for diffraction geometry and definition of angles). The detector on SALSA is a 2D-position sensitive detector, covering 9.5° in 2θ with an average channel width of 0.447°. It was positioned at $2\theta = 88.5°$ for Al measurements and at $2\theta = 93.4°$ for steel plate measurements. The rotation table of SALSA was positioned either at ω=44.25° or -46.7° for the Al measurements and at ω=46.7° and -43.3° respectively for measurements of the steel part. At these angular positions the principal axis directions of the strain tensor lied in the direction of the scattering vector, which is the bisecting angle between incoming and diffracted beam. This choice was made on the assumption that the principal axes directions correspond to symmetry axes of the sample.

As diffraction angles are distinct for aluminum and steel, there is no problem of deconvolution which would have been due to overlapping. Note that in the prior investigations of MPW of AA1050/DP450, $FeAl_3$ intermetallic compound (IMC) was locally identified at the AA1050/DP450 interface **[22].** The effect of this IMC, whose formation has very likely generated stresses at the joint interface, is not considered in first approximation. Also note that no shift or split of the peak for Fe was observed despite the presence of both ferritic and martensitic phases in the DP450 steel. The observed Fe peak indeed results from the convolution of both ferrite and martensite peaks. The martensite has very likely a composition close to that of ferrite, which must have entailed only slight offsets in lattice parameters. The smallest nominal gauge volume defined by SALSA instrument, i.e.

$0.6\times0.6\times2$ mm^3 full width at half maximum, was considered in the present work to obtain the highest possible resolution close to the aluminum AA1050/DP450-steel interface. The instrumental gauge volume (IGV) is defined by radial focusing collimators **[29].** By dividing the IGV in small steps (i.e. 0.1 mm) into the sample, and across the interface respectively, the lateral resolution can be improved up to a factor of ~1/18 compared to the width of the IGV. Indeed, the sampled gauge volume (SGV), which is the intersection of the IGV with the sample material, is smaller than the IGV. Additionally, due to the pyramidal shaped intensity profile within the IGV combined with the absorption of the material, the center of gravity (COG) of the SGV becomes closer to the surface than the center of gravity of its footprint. This COG is taken as the actual measuring point. This procedure enables to obtain measuring points as close as ~70 μm to the interface, despite a much larger instrumental gauge volume used in the experiment.

Diffraction peaks were acquired such that a given number of neutrons was counted and the count time was adapted automatically. These were 800 counts for the iron peaks and 1400 counts for the aluminum peaks. This procedure ensures equal quality of data even at positions close to the surface where the intensity drops due to the smaller sampled gauge volume (SGV). The longitudinal and transverse components were measured in transmission mode while the normal component was obtained in reflection mode (Fig. 3).

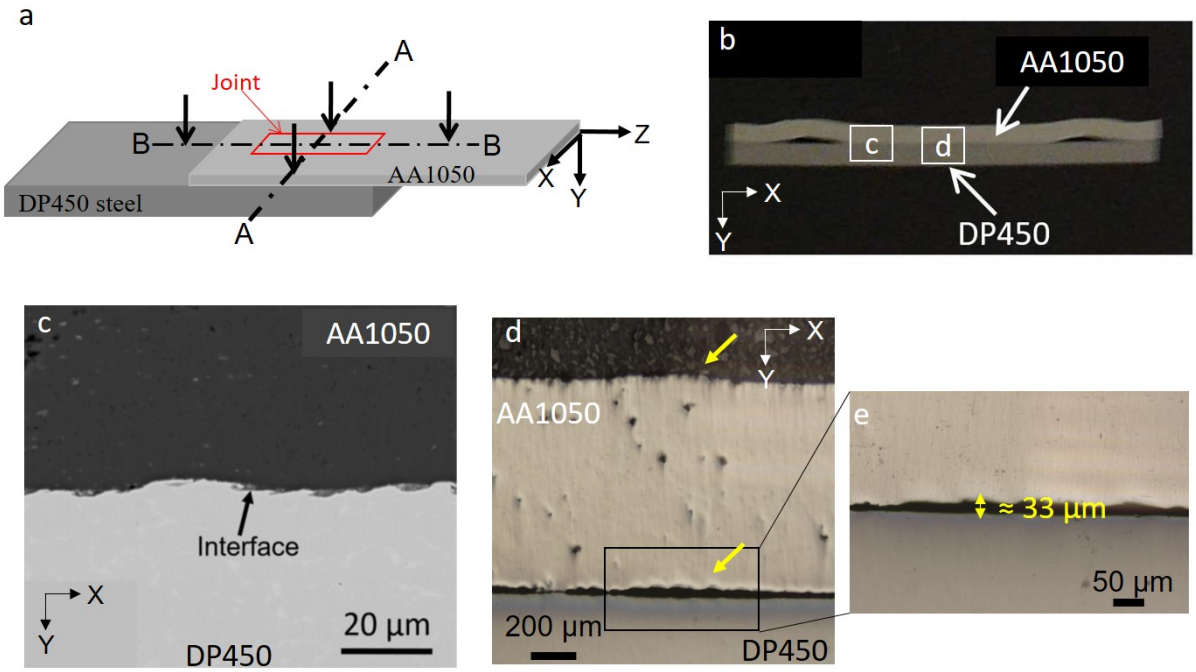

Fig. 2: (a) Schematic illustration of the welding configuration and welded zone. (b) Transverse section indicating the location of the micrographs shown in (c) and (d) of the weld along A-A marked in (a). (c) Scanning electron microscopy (SEM) images showing a wavy interfacial zone in the welded area obtained from section A-A and (d and e) light micrographs of the plates revealing the central unwelded area from section A-A. Note that (X,Y,Z)=(0,0,0) corresponds to the Al – steel interface at the intersection of A-A and B-B planes.

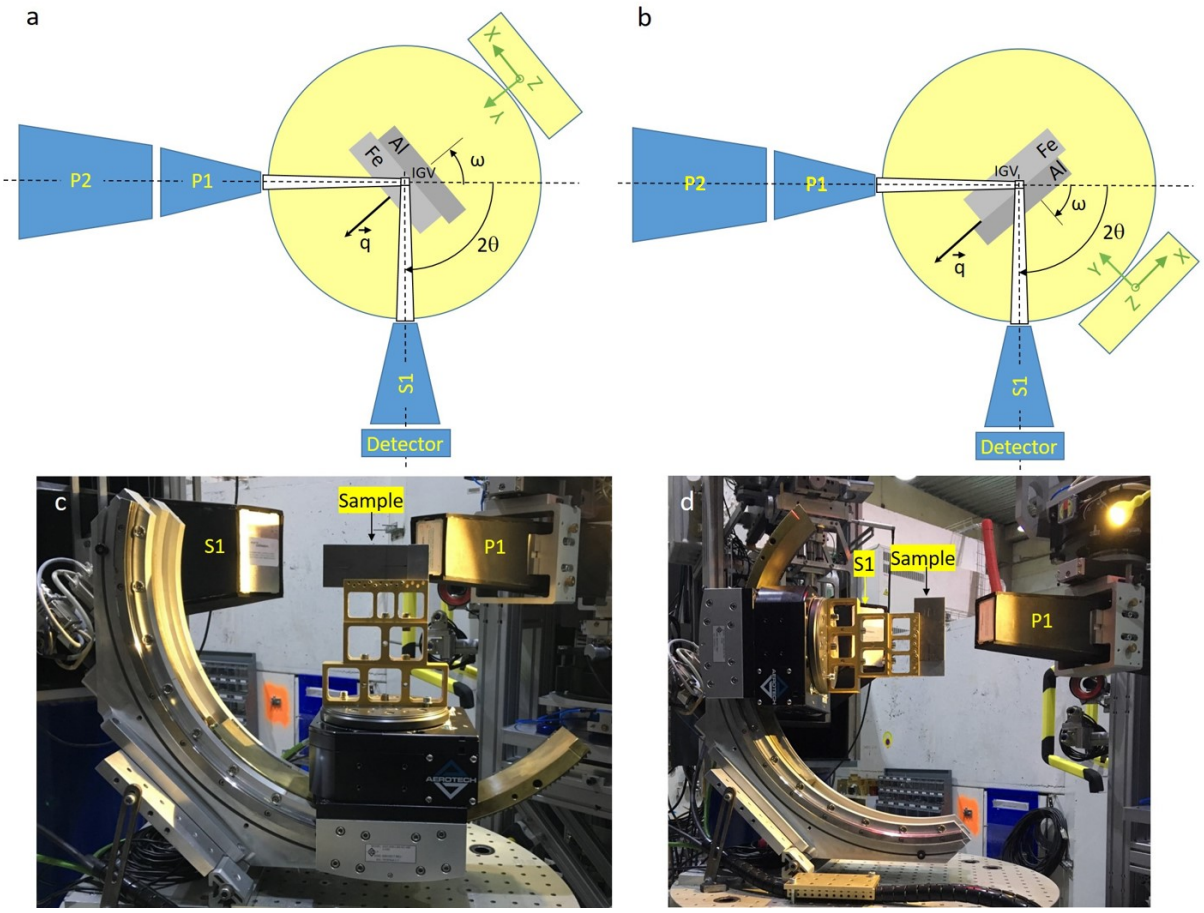

Fig. 3: (a) Reflection mode for measurement of the normal strain component. (b) Transmission mode for transverse and longitudinal components. P1 and P2 are the primary radial focusing collimators and S1 is the secondary collimator. P2 defines a 2 mm FWHM (Full Width at Half Maximum) beam height and P1 and S1 define a horizontal cross section of 0.6×0.6 mm^2 FWHM. IGV stands for instrumental gauge volume and $\vec{q}$ for the scattering vector. The photography in (c) shows the configuration for normal measurement for all Lines, for transverse measurement for Line 3, and for longitudinal measurements for Lines 1 and 2. The photography in (d) shows the configuration after the physical rotation of the sample without changing the beam, used for the transverse measurement along Lines 1 and 2, and the longitudinal measurement along Line 3. The collimator visible on the right-hand side is P1 and S1 is to the left of the sample in (c) and (d).

Measurements were performed such that the IGV was scanned across the interface in 0.1 mm steps, which corresponds approximately to a 15^{th} of its diagonal. This way the volume of the SGV changes successively, thus allowing to resolve the residual stress gradients near the interface. Scans were performed in the sample thickness direction for the three principal axis directions, by orienting the sample accordingly as described above (Figs. 3 and 4). Three lines

have been measured: Line 1 at the center of the welded spot through the unwelded zone (Fig. 4a and c), Line 2 across the long weld interface (Fig. 4a and c) and Line 3 across the short joint interface (Fig. 4b and d). In order to determine stress free reference values, two cubes of 4×4×2 mm^3 volume were prepared from the parent materials.

Since a strain scanning diffractometer is not designed to determine absolute lattice spacings, but is optimized to resolve small shifts in diffraction peak positions, the following equation 1 is used to calculate strain. It follows directly from Bragg's law using the definition of strain:

$$\varepsilon = \frac{\sin(\theta_0)}{\sin(\theta)} - 1 \qquad \text{[Eq. 1]}$$

where ε is strain, θ the diffraction angle obtained from the measurements and θ_0 the diffraction angle of the reference sample measurements. d and d_0 are the corresponding lattice spacings.

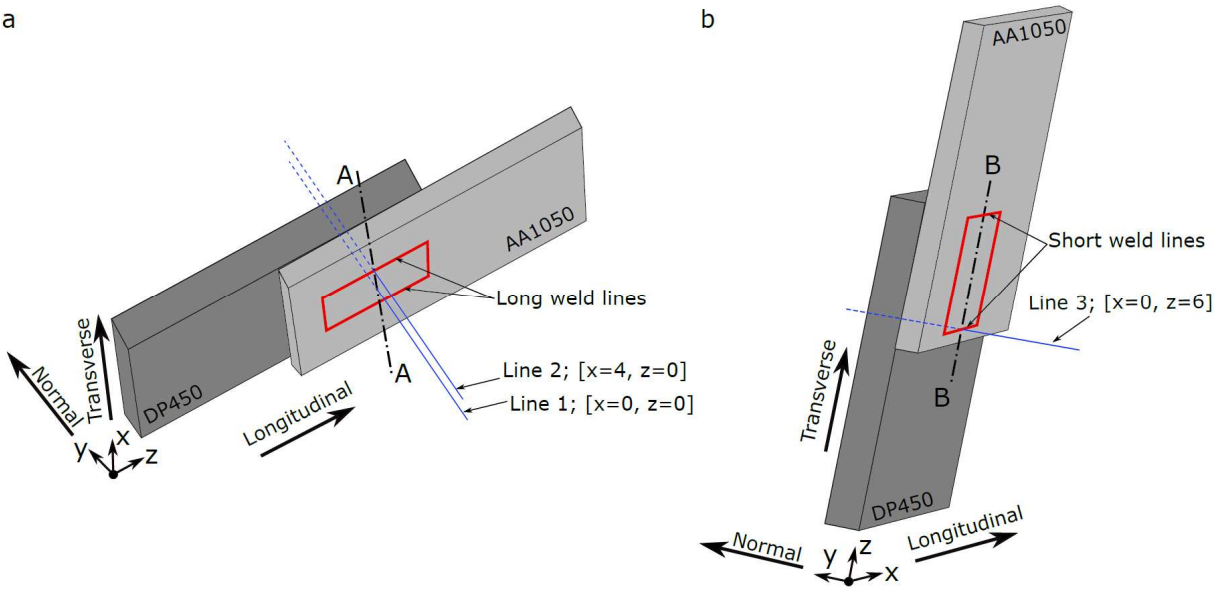

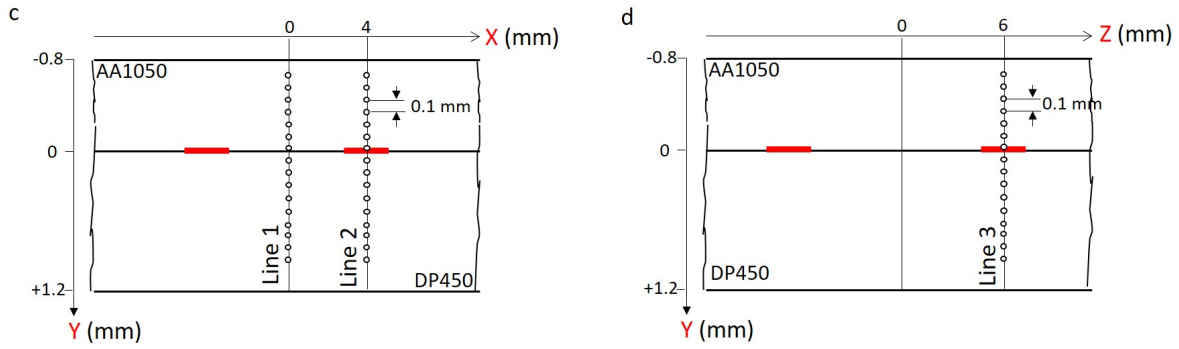

Fig. 4: Schematic 3D illustrations showing the stress components with respect to the residual stresses measurement along (a) Lines 1 and 2 and (b) Line 3. The red lines in (a) and (b) indicate the weld lines. X = 0 and Z = 0 define the Line 1, which goes through the weld center. Y = 0 defines the interface while the positive Y corresponds to the normal distance into the steel from the interface, while the negative Y corresponds to the normal distance into the Al from the interface. Locations of the diffraction points, that is the centroid positions of the instrumental gauge volume (IGV), are indicated in (X-Y) plane along Lines 1 and 2 in (c) and in (Y-Z) plane along Line 3 in (d).

The measurements were post processed using LAMP software **[30]** by fitting a Gaussian distribution function to the peak profiles. Intensities were normalized by the count time. The obtained intensity profile is a measure for the size of the SGV and therefore for its position. The COG for each step, i.e. the measuring location, is precisely determined using the in-house code "PS-Fit" written in Mathcad. A paper explaining the model used in the program PS-Fit is in preparation **[31].** The same program is used to correct for pseudo peak shift, caused by the fact that the sampled gauge volume is displaced with respect to both the instrument center to which angular calibration is performed and the wavelength distribution within the primary beam. The amount of this peak shift was determined by a reference measurement in which a 0.3 mm thin iron foil was scanned in reflection and transmission geometry. For a better understanding of this effect, the reader is referred to the detailed explanations provided in previous papers **[10, 29, 32].**

The individual strain components were computed using Bragg's law and the residual stresses calculated by means of the Hooke's law [Eqs. 2-4] for the three orthogonal directions.

$$\sigma_{xx} = 2 \times \mu^{hkl} \times \varepsilon_{xx} + \lambda^{hkl} \times (\epsilon_{xx} + \epsilon_{yy} + \epsilon_{zz}) \qquad \text{[Eq. 2]}$$

$$\sigma_{yy} = 2 \times \mu^{hkl} \times \varepsilon_{yy} + \lambda^{hkl} \times (\epsilon_{xx} + \epsilon_{yy} + \epsilon_{zz}) \quad \text{[Eq. 3]}$$

$$\sigma_{zz} = 2 \times \mu^{hkl} \times \varepsilon_{zz} + \lambda^{hkl} \times (\epsilon_{xx} + \epsilon_{yy} + \epsilon_{zz}) \quad \text{[Eq. 4]}$$

where λ^{hkl} and μ^{hkl} are Lamé's constants defined in Eqs. 5 and 6 for the considered lattice planes.

$$\lambda^{hkl} = \frac{\nu^{hkl} \times E^{hkl}}{(1 + \nu^{hkl}) \times (1 - 2 \times \nu^{hkl})} \quad \text{[Eq.5]}$$

$$\mu^{hkl} = \frac{E^{hkl}}{2 \times (1 + \nu^{hkl})} \quad \text{[Eq. 6]}$$

where ε_{xx}, ε_{yy}, ε_{zz} are transverse, normal and longitudinal strain components, respectively (case of Line 2 here (see Fig. 4a)). ν^{hkl} is the crystallographic Poisson's coefficient and E^{hkl} is the Young's modulus for the selected family of planes. ν^{311} is equal to 0.35 for Al and ν^{211} to 0.28 for Fe; E^{311} is equal to 70.2 GPa for Al and E^{211} to 225.5 GPa for Fe **[33]**. For stress calculation we consider all the measuring positions from all three directions. Moreover, the residual stresses are interpolated for those measuring points where there are no data in any of those corresponding directions. So, the number of measuring points in stress calculation can be the sum of the number of all locations or less, if points have been measured at exactly the same coordinate in all three directions, or at the surface where some points cannot be calculated.

3. Results: residual stresses

Fig. 5 and Fig. 6 show the normal-, transverse- and longitudinal- residual stress components (see Figs. 4a and b for the definition). Note that residual stresses have a low magnitude on the Al side. This is very likely due to the low strength of the selected Al grade. In addition, the profiles of residual stresses are asymmetrical on both sides of the interface. The residual stresses will be explained in the following sections based on the identified interface features of the assembly, i.e. short or long welded interface and unwelded zone.

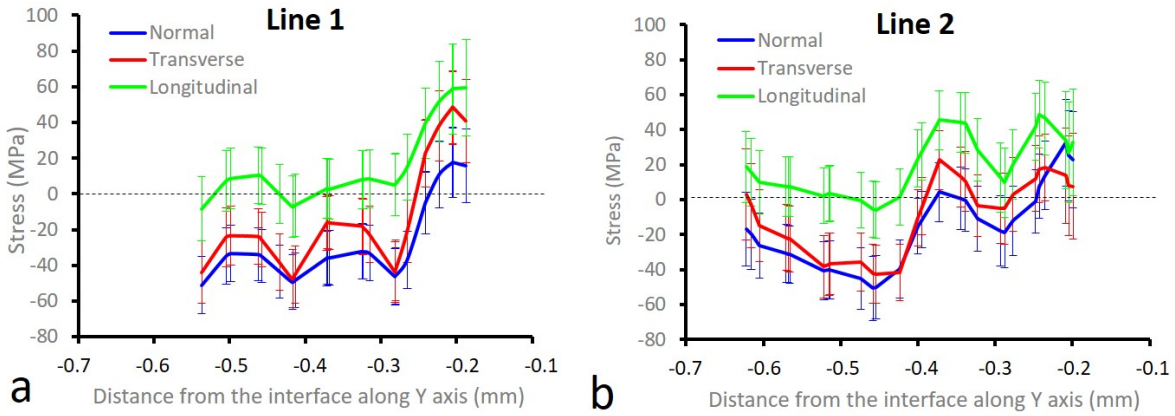

Figure 5: Normal, transverse and longitudinal components of residual stresses for the Al sheet at (a) unwelded position [Line 1] and (b) welded position [Line 2]. The actual measuring positions (that is the distances from the interface) are the coordinates of the centre of gravity of the sampled gauge volumes obtained from "PS-Fit" for pseudo peak shift correction. Y is the thickness direction (Figs. 2 and 4).

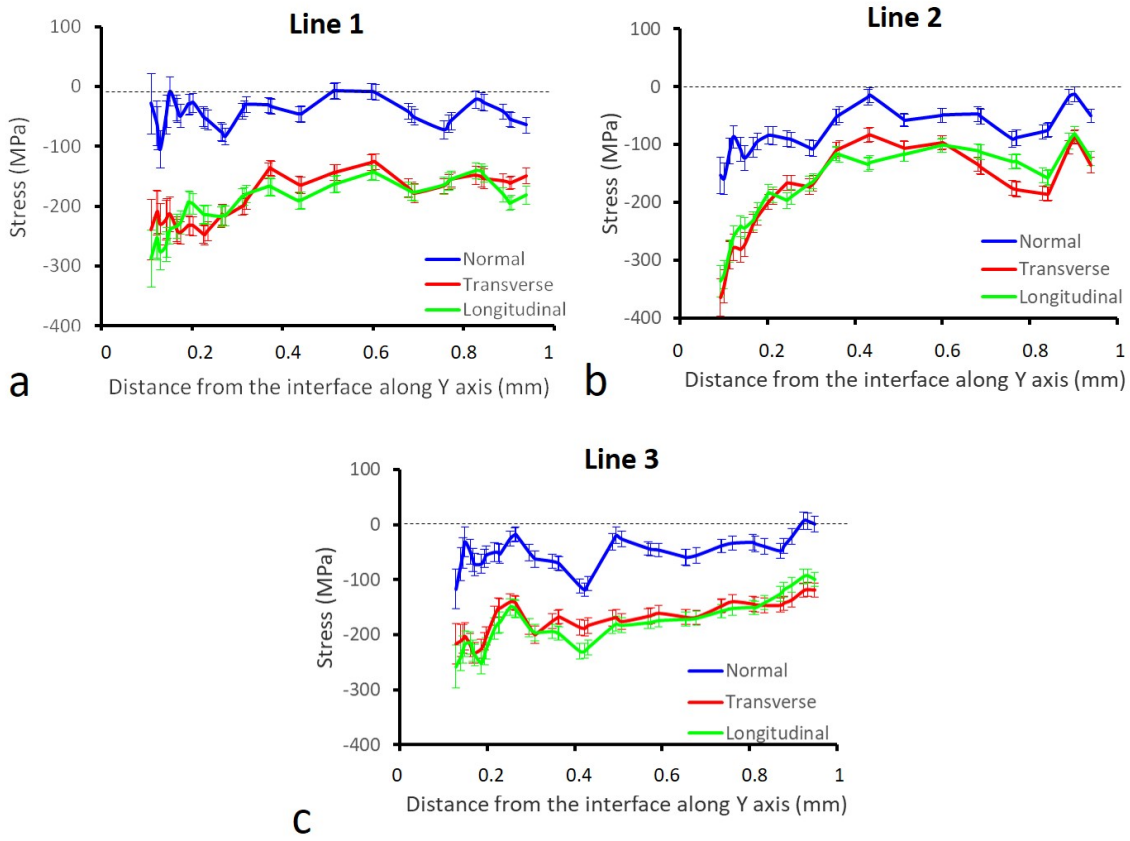

Figure 6: Normal, transverse and longitudinal components of residual stresses for the steel sheet at (a) unwelded position along Line 1, and welded positions along (b) Line 2 and (c)

Line 3 (c). The actual measuring position (that is the distances from the interface) is the coordinate of the centre of gravity of the sampled gauge volume obtained from "PS-Fit" for pseudo peak shift correction. Reminder: Y is the thickness direction (Figs. 2 and 4).

It was not practical to align a non-uniform sample like this one in all three orientations with a precision better than ~0.1 mm. But fitting of the intensity profile as part of the pseudo peak shift correction allows the determination of the interface position with a precision of typically 10 to 25 μm. The measuring positions have then been recalibrated to the position of the interface determined in the described way. Near the interface the coordinates of the measuring points have been calculated as the COG of the SGV. They are therefore denser than the original step of 0.1 mm of the scan. As a result, the measuring points of the three strain components do not overlay any more. Therefore, for stress calculation, missing points had been linearly interpolated. This explains the bigger number of points in the graphs than in the measuring plan of Fig. 4.

3.1. Unwelded zone (residual stress measurement at Line 1)

The unwelded zone located at the center of the assembly (X=0, Y=0, Z=0) cannot be considered as a reference state. Indeed, the impact generated during the process led to bending of the plates (see yellow arrows in Fig. 2d). In this location a gap of about 33 μm is found between the aluminum and steel plates (Fig. 2e). The residual stresses found here are generated by bending of the plates.

Tensile stresses are found close to the gap in aluminum. They are of the same magnitude, between 15 and 60 MPa, as in the welded part but decrease more rapidly, i.e. the residual stresses are higher mainly within the 0.3 mm from the interface (Figs. 5a and b). Further away from these 0.3 mm, stresses remain constant at levels of around -40 MPa (compression) for the normal and transverse components and 0 MPa for the longitudinal one.

In the steel plate a slight gradient of compressive stresses up to -250 MPa and -290 MPa for the transverse and longitudinal component is observed within the first 0.35 mm from the interface. Then stresses remain constant around -180 MPa. (Fig. 6a). The normal stress component remains very low.

3.2. Long welded line (residual stress measurement at Line 2)

On the Al side (Fig. 5b), residual stresses below the welded line have a similar trend as in the unwelded location (Fig. 5a). But tensile stresses remain over a larger depth for the first 0.4 mm from the interface compared to 0.3 mm. Once again, close to the interface, longitudinal stresses are higher than the normal and transverse ones. The maximum tensile residual stresses in longitudinal, normal and transverse directions reach 60, 40 and 20 MPa, respectively, close to the interface.

On the steel side (Fig. 6b), a more significant gradient of compressive stresses than in the unwelded part is observed for a distance of 0.43 mm from the interface. Maximum values are found to be -325 MPa and -375 MPa in longitudinal and transverse direction. Stresses remain compressive for the entire thickness under the welded line at levels of about -150 MPa for the transverse and longitudinal component. The normal component remains very low.

3.3. Short welded line (residual stress measurement at Line 3)

Due to limited beam time, analysis of residual stresses for the short welded line on the Al side could not be performed. However, the evolution of residual stresses in this area is likely intermediate between those obtained for the unwelded zone (see Line 1) and the long welded line (see Line 2).

On the steel side (Fig. 6c), residual stresses are everywhere compressive along this short weld. Similarly to the long welded section, normal residual stresses are smaller in absolute values than longitudinal and transverse residual stresses. In all directions, a gradual

increase of these compressive residual stresses is observed from a distance of 0.95 to 0.12 mm from the interface. Nevertheless, this stress increase is of low magnitude, i.e. roughly 125 MPa for normal, longitudinal and transverse residual stresses. This increase is comparatively lower than in the long welded line, i.e. 125 MPa for normal, 250 MPa for longitudinal and 300 MPa for transverse. In this area, the compressive residual stresses are less pronounced and their maximum in absolute values smaller (125 MPa for normal, 260 MPa for longitudinal and 225 MPa for transverse) than in the long welded line on Line 2 (160 MPa for normal, 325 MPa for longitudinal and 375 MPa for transverse).

Before discussing the results obtained by neutron diffraction, let us summarize them:

(i) Residual stresses on Al side become tensile close to the interface but remain very low. Their amplitude is similar at the unwelded and welded areas, but their tensile feature is evidenced over a greater distance from the interface in the case of welded lines. The longitudinal stresses are greater than the normal and transverse stresses.

(ii) Residual stresses on steel side are compressive for all distances from the welded or unwelded interface. They have a higher magnitude close to the interface ordered as follows: long welded line, short welded line and unwelded zone. The longitudinal and transverse components of residual stresses are similar.

4. Discussion

4.1 Magnitude and asymmetry of residual stresses along the joint lines

The absolute values of residual stresses (Fig. 5) remain slightly below or close to the magnitude of the yield strength of Al (around 40 to 100 MPa **[16]**) on the Al side. On the steel side, the magnitude of the maximum compressive residual stresses (Fig. 6) is on the order of magnitude of the yield strength of DP450 steel (290-340 MPa **[16]**). The difference in yield

strengths between both materials justifies that the maximum residual stresses (in absolute values) of pure Al are significantly lower compared to those in DP450 steel.

On the steel side, the residual stresses are compressive. The normal residual stresses are higher along the welded Lines 2 and 3 than along the unwelded Line 1. This is consistent with the impact phenomena. Besides, welding occurs following the impact (Line 2 and Line 3). This welding mechanism made the steel constrained with high magnitude of compressive (i.e. low values) residual stresses in the transverse and longitudinal directions. The longitudinal and transverse residual stresses are in-plane stresses and those are interchangeable for the long and short weld lines (see Figs. 4a and b). Since the weld shape is rectangular, the residual stresses were accommodated in longitudinal and transverse directions and present a similar order of magnitude. The normal stresses are generated mainly by the impact, and they are an out of plane component. Thus, a low magnitude of residual stresses in the normal directions was obtained.

Given the asymmetric shape of the weld spot (Figs. 1 and 2a), some asymmetrical residual stress profiles are measured on the steel side within the long (see Line 2) and short (see Line 3) welded lines (Figs. 6b and c). Larger residual stresses were measured on the long welded line, i.e. it is the most critical part of the weld (Figs. 5 and 6).

4.2 Sources of residual stresses

High strain and high strain rate during welding - Since AA1050 and DP450 steel experience high plastic strain and strain rate during magnetic pulse welding, some plastic yielding occurs at their welded and unwelded interfaces, thus generating residual stresses. Indeed, the used materials are more or less sensitive to strain and strain rate since they can more or less easily accommodate the deformation generated by the impact during welding, according to their crystal lattice, the crystal orientation of the grains (which can lead to

heterogeneous plastic flow/deformation according to the grains) and their deformation modes (work hardening, twinning, slipping etc). The deformation mechanisms at the microstructural level significantly influence the magnitude and the distribution of residual stresses in the materials.

Hump forming - The deep drawing of a hump on the aluminum flyer sheet must also have generated residual stresses on the aluminum side. However, the hump has then been flattened out during the welding process. Therefore, the residual stresses resulting from the bending process are completely ignored. Thus, there is no evidence of tensile residual stresses in the outside of the Al plate and compressive residual stresses in the inside surface of the Al plate. Instead, tensile residual stresses are measured on the inside of the aluminum side (i.e. close to the interface) at both unwelded and welded lines.

Thermal expansion – Thermal stresses induced during the process might be a source of residual stresses. Indeed, the localized heating generated by the impact **[23]** very likely entailed small thermal expansion of both AA1050 and DP450 steel over small thicknesses. Thermal expansion is given by the product of the coefficient of thermal expansion (CTE) and temperature interval. The CTE of AA1050 and DP450 steel are 23.8×10^{-6} $°C^{-1}$ and 12.3×10^{-6} $°C^{-1}$, respectively. The difference of CTE will cause different magnitudes of residual stresses from either side of the joint interface; besides the thermal expansion should occur over a larger distance on the steel side, given the respective thermal diffusivities of both Al (98 mm^2/s) and steel (21 mm^2/s). However, AA1050-galvanized DP450 steel MPW joint obtained under similar conditions as in the current study reached a temperature during the process below the Zn solidus temperature (around 419°C) as no solidification defects were reported **[22,23]**. Thus, the global thermal expansion in the current work must be of low magnitude on both sides of the welded interface. Thermal expansion can therefore be excluded as a predominant factor for the generation of residual stresses.

Intermetallic compounds – The formation of local micrometric $FeAl_3$ intermetallic compounds (IMC) **[22]** on Al side at the joint interface plays very likely a minor role on residual stresses. By considering the crystallography of $FeAl_3$ and Al, the formation of $FeAl_3$ IMC should entail a volume increase of about 57 times with respect to the Al matrix. This should thus lead to compressive stresses in AA1050. However, since the formation of these small amounts of intermetallics are extremely local and discontinuous, the residual stresses generated by their formation must be of low magnitude, compared to those generated by the impact. This argument is consistent with the fact that residual stresses on Al side are tensile close to the joint interface (Fig. 6b). It is also reinforced by the fact that the microstructure (not shown here) is homogeneous in both materials except over a distance of about 50 µm on either side of the interface where it is more or less distorted because of high deformation, as shown in other papers **[34,35]**. This distance is far smaller than the 400 µm large zone over which there is an increase of residual stresses (Figs. 5 and 6). The microstructure is homogenous over the whole sample except a 50 micrometres thick layer next to the interface. Therefore we could apply the d0 value obtained from the base material in the far field for the investigated areas (Figs. 5 and 6).

4.3 Comparison of residual stresses in MPW to residual stresses in explosive welding, explosive treatment and shot peening

An analogy of MPW is firstly done with explosive welding. It is interesting to note that, as in the current study, the flyer can present some tensile stresses while the clamped piece is characterized by compressive stresses like in niobium – steel explosive welds **[11]**. In Al-Cu-Al explosive welds, the flying sheet (Al) was also shown to be subjected to tensile residual stresses **[2]**. The authors explained this result by the explosion waves which moved in the direction of explosion. They also added that the tensile stresses then transmit to the copper

as soon as it becomes in contact with Al. The difference of residual stresses distribution in this work compared to the present study may be due to the material nature, to the weld geometries etc. In addition and conversely to our study, in the case of Ti/Al explosive weld **[3]**, the flyer, which is Ti Grade 2, presents compressive residual stresses. In the Ti plate, close to the joint interface, compressive twinning was mainly observed compared to tensile twinning and slipping. No significant residual stress was observed in Al because of the accommodation of large strains by a fcc lattice (Al) due to a higher number of slip systems than in the hcp structure (Ti). Multiple sliding systems allow easier plastic deformation reducing the amount of energy being accumulated in the form of elastic internal stresses. This proves once again that there is no obvious rule to say that the flyer and stationary plates will have certain types of residual stresses irrespective of the materials.

The fatigue life and the crack initiation and propagation are normally affected by the mechanical properties due the presence of nonnegligible residual stresses in the welded joints [36]. These behaviors are highly complex and specific to each situation due to the presence of various residual stress components, to the different material behaviors (from low- to high strength steels, and aluminum) and various types of fatigue loading conditions. It is worth to check this subject on a case by case basis. However, relieving stresses or introducing compressive residual stresses is beneficial to improve the fatigue life and mitigate the crack propagation behaviors [37-38]. For example, explosive treatment or shot peening is used [37-39] to relief residual stressess and introduce compressive residual stresses via the mechanisms of impact and/or shock. Since these two processes have some impact behaviors similar to MPW and since the residual stress on steel is compressive after MPW, a comparison is made in Table 2 between MPW and these two processes.

Table 2: A comparison between MPW, explosive treatment and shot peening

Process	MPW	Explosive treatment	Mechanical shot peening
Loading	Single	Cyclic shock wave	Cyclic impacts
Stain rate	10^7 s^{-1} at the interface [40]	10^3-10^5 s^{-1} [41, 42]*	10^5-10^6 s^{-1} [43]
Process duration	9.5 µs for MPW for the considered joint [22]	About 500 µs [39]	up to 60 min [44]
Impacting Speed	Al flyer sheet speed of 514 m/s at the onset of impact in our MPW [22]	No impact. Explosive buffer is placed on the workpieces and exploded	20 – 150 m/s for 0.25 – 1 mm diameter spherical shots or 5 – 15 m/s in surface mechanical attrition treatment for 5 – 10 mm diameter spherical shots [45]

*The strain rate reported is based on explosive welding experimental literature

5. Conclusions

The originality of the present investigation lies in the fact that residual stresses were analyzed for the first time for a dissimilar AA1050 – DP450 steel planar spot magnetic pulse weld using nondestructive neutron diffraction technique. Moreover, an advanced characterization protocol is applied to solve tri-axial residual stresses profiles near the interface by applying an analytical model to correct for pseudo strain, which arise in near surface or interface diffraction measurements. The main findings of this work are summarized below:

- Close to the joint interface, compressive residual stresses were detected on the steel side. Conversely, tensile residual stresses were measured on the Al side. These residual stresses essentially result from high strains and strain rates due to impact during welding.
- Close to the joint interface, on the Al side, the longitudinal stresses are the largest while on steel side, longitudinal and transverse residual stresses are dominant with a similar magnitude.
- The asymmetrical shape of the spot joint leads to residual stresses with a lower magnitude along the short joint line of the weld for the steel side.

Data statement

The original neutron diffraction data reported in this publication is accessible from Institut Laue-Langevin (ILL) data repository at: doi:10.5291/ILL-DATA.1-04-163

Experiment title: Residual stress measurement in Al/steel joint produced by magnetic pulse welding

Instrument: SALSA (Strain Analyzer for Large and Small scale engineering Application).

Acknowledgments

The authors acknowledge the international Neutron Source at Institut Max von Laue – Paul Langevin (ILL) for the provision of beamtime for the experiment 1-04-163. TS acknowledges F.R.S.-FNRS, (Belgium) for his postdoctoral fellowship at UCLouvain.

References

[1] Hensel J, Nitschke-Pagel T, Tchoffo Ngoula D, Beier H-Th, Tchuindjang D, Zerbst U. Welding residual stresses as needed for the prediction of fatigue crack propagation and fatigue strength. Engin Fracture Mechanics 2018;198:123-141

[2] Sedighi M, Honarpisheh M. Experimental study of through-depth residual stress in explosive welded Al-Cu-Al multilayer. Mater and Design 2012;37:577-581

[3] Fronczek DM, Saksl K, Chulist R, Michalik S, Wojewoda-Budka J, Sniezek L, Wachowski M, Torzewski J, Sulikova M, Sulova K, Lachova A, Fejercak M, Daisenberger D, Szulc Z, Kania Z. Residual stresses distribution, correlated with bending tests, within explosively welded Ti gr. 2/A1050 bimetals. Mater Charact 2018;144:461-468

[4] Jang J, Son D, Lee Y-H, Choi Y, Kwon D. Assessing welding residual stress in A335 P12 steel welds before and after stress-relaxation annealing through instrumented indentation technique. Scripta Mat. 2006;48:743-748

[5] Cai Z, Huang X. Residual stress reduction by combined treatment of pulsed magnetic field and pulse current. Mater Sci Engin A 2011;528:6287-6292

[6] Lai HH, Cheng HH, Lee CY, Lin CM, Wu W. Effect of shot peening time on δ/γ residual stress profiles of AISI 304 weld. J Mater Proc Technol 2020;284:116747

[7] Rossini NS, Dassisti M, Benyounis KY, Olabi AG. Methods of measuring residual stresses in components. Mater Design 2012;35:572-588

[8] Guo J, Fu H, Pan B, Kang R. Recent progress of residual stress measurement methods: a review. Chinese Journal of Aeronautics 2019; DOI: 10.1016/j.cja.2019.10.010

[9] Withers PJ. Mapping residual and internal stress in materials by neutron diffraction. C.R. Physique 2007;8:806-820

[10] Jimenez-Mena N, Sapanathan T, Drezet JM, Pirling T, Jacques PJ, Simar A. Residual stresses of friction melt bonded aluminium/steel joints determined by neutron diffraction. J Mater Proc Tech. 2019;266:651-661

[11] Taran YV, Balagurov AM, Sabirov BM, Davydov V, Venter AM. Neutron diffraction investigation of residual stresses induced in niobium-steel bilayer pipe manufactured by explosive welding. Mater Sci Forum 2013;768-769:697-704

[12] Li C, Fan D, Yu X, Huang J. Residual stress and welding distorsion of Al/steel butt joint by arc-assisted laser welding-brazing. Trans Nonferrous Met Soc China 2019;29:692-700

[13] Karolczuk A, Kluger K, Kowalski M, Zok F, Robak G. Residual stresses in steel-titanium composite manufactured by explosive welding. Mater Sci Forum 2012;726:125-132

[14] Karolczuk A, Kowalski M, Kluger K, Zok F. Identification of residual stress phenomena based on the hole drilling method in explosively welded steel-titanium composite. Arch Metall Mater 2014;59:1129-1133

[15] Ueda Y, Murakawa H, Ma NX. Measuring method for residual stresses in explosively clad plates and a method of residual stress reduction J. Eng Mater Technol 1996;118:576-582

[16] Granta Edupack Software, Granta Design Limited, Cambridge, UK, 2020

[17] Gan WM, Hofmann M, Ventzke V, Randau C, Huang YD, Kriele A, Brokmeier HG, Mueller M. Microstructure and residual stress in rotary friction welded dissimilar metals of AA7020 aluminium alloy with 316L steel. Mater Sci Forum. Trans Tech Publ 2017:572-577

[18] Wang H, Wang Y. High –velocity impact welding process: a review. Metals 2019;9(2):144

[19] Kapil A, Sjarma A. Magnetic pulse welding: an efficient and environmentally friendly multi-material joining technique. J Clean Prod 2015;100:35-38

[20] Miranda RM, Tomas B, Santos TG, Fernandes N. Magnetic pulse welding on the cutting edge of industrial applications. Soldag Insp Sao Paulo 2014;19(01):69-81

[21] Aizawa T, Kashani M, Okagawa K. Application of magnetic pulse welding for aluminum alloys and SPCC steel sheet joints. Weld J 2007;86:119-s-124-s

[22] Avettand-Fènoël MN, Khalil C, Taillard R, Racineux G. Effect of steel galvanization on the microstructure and mechanical performances of planar magnetic pulse welds of aluminum and steel. Met Mat Trans A 2018;49:2721-2738

[23] Avettand-Fènoël MN, Marinova M, Taillard R. Atomic scale characterization of a pure Al – galvanized steel spot magnetic pulse joint interface. Mater Character 2019;153:251-260

[24] Raoelison RN, Buiron N, Rachik M, Haye D, Franz G, Habak M. Study of the elaboration of a practical weldability window in magnetic pulse welding. J Mater Proc Technol 2013;213:1348-1354

[25] Manogaran AP, Manoharan P, Priem D, Marya S, Racineux G. Magnetic pulse spot welding of bimetals. J Mat Proc Technol 2014;214:1236-1244

[26] Pirling T, Bruno G, Withers PJ. SALSA – A new instrument for strain imaging in engineering materials and components. Mat Sci Eng A 2006;437:139-144

[27] Jacques PJ, Furnemont Q, Godet S, Pardoen T, Conlon K, Delannay F. Micromechanical characterization of TRIP-assisted multiphase steels by in situ neutron diffraction. Phill Mag 2006;86:2371-2392

[28] Chobaut N. Measurements and modelling of residual stresses during quenching of thick heat treatable aluminium components in relation to their precipitation state, EPFL

[29] Pirling T. Precise analysis of near surface neutron strain imaging measurements, Procedia Engin 2011;10:2147-2152

[30] Richard D, Ferrand M, Kearley GJ. Analysis and Visualisation of Neutron-Scattering Data. J. Neutron Research 1996;4:33-39. DOI: 10.1080/10238169608200065

[31] Pirling T., Analytical model and practical method for the correction of pseudo peak shift occuring on monochromatic neutron strain scanning diffractometers, In preparation

[32] Bruno G, Fanara C, Hughes DJ, Ratel N. Procedures for interface residual stress determination using neutron diffraction: Mo-coated steel gear wheel. Nuclear Instruments and Methods in Physics Research Section B: Beam Interactions with Materials and Atoms 2006;246 :425-439.

[33] Hutchings MT, Withers PJ, Holden TM, Lorentzen T. I,troduction to the characterization of residual stress by neutron diffraction. CRC press, Boca Raton, USA, 2005

[34] Liu BC, Palazotto AN, Nassiri A, Vivek A, Daehn GS. Experimental and numerical investigation of interfacial microstructure in fully age-hardened 15-5 PH stainless steel during impact welding. J Mater Sci 2019;54:9824-9842

[35] Raoelison RN, Sapanathan T, Buiron N, Rachik M. Magnetic pulse welding of Al/Al and Al/Cu metal pairs: consequences of the dissimilar combination on the interfacial behavior during the welding process. J Manuf Proc 2015;20:112-127

[36] G. Glinka, "Effect of residual stresses on fatigue crack growth in steel weldments under constant and variable amplitude loads," in Fracture Mechanics: Proceedings of the Eleventh National Symposium on Fracture Mechanics: Part I, 1979: ASTM International.

[37] Liu W.C., et al., Improvement of fatigue properties by shot peening for Mg–10Gd–3Y alloys under different conditions. Materials Science and Engineering: A, 2011. 528(18): p. 5935-5944.

[38] Trung PQ, Win KN, Butler D. Effect of shot peening process on the fatigue life of shot peened low alloy steel. J Eng Mater Tech 2018;140:1-7

[39] Zhang J, Liu K, Zhao K, Li X, Liu Y, Zhang K. A study on the relief of residual stresses in weldments with explosive treatment. International Journal of Solids and Structures 42 (2005) 3794–3806

[40] Zhang Y, Babu SS, Prothe C, Blakely M, Kwasegroch J, LaHa M, Daehn GS. Application of high velocity impact welding at varied different length scales. J Mater Proc Technol 2011;211:944-952

[41] Guo YS, Chen PW, Arab A, Zhou Q, Mahmood Y. High strain rate deformation of explosion welded Ti6Al4V/pure titanium. Defence Technology 2020;16(3):678-688

[42] Maloy SA, Gray GT, Cady CM, Rutherford RW, Hixson RS. The influence of Explosive-Driven “Taylor-Wave” Shock prestraining on the Structure/property Behavior of 304 Stainless Steel. Met Mat Trans A 2004;35:2617-2624

[43] Buvaraghan B, Srinivasan SM, Maffeo B, Prakash O, Analytical solution for single and multiple impacts with strain-rate effects for shot peening. CMES 2010;1550(1):1-22

[44] Liu YG, Li MQ, Liu HJ. Nanostructure and surface roughness in the processed surface layer of Ti-6Al-4V via shot peening. Mater Charact 2017;123:83-90

[45] Ortiz AL, Tian JW, Shaw LL, Liaw PK. Experimental study of the microstructure and stress state of shot peened and surface mechanical attrition treated nickel alloys. Scripta Mater 2010;62:129-132